Macromolecules

Article

pubs.acs.org/Macromolecules

Role of the Comonomeric Units in Reaching Linear Backbone, High Solid-State Order and Charge Mobilities in Heptacyclic Arene-Based Alternating Copolymers

Tien-Hsin Lee, Kuan-Yi Wu, Tai-Yen Lin, Jhong-Sian Wu, Chien-Lung Wang,* and Chain-Shu Hsu*

Department of Applied Chemistry, National Chiao Tung University, 1001 Ta Hsueh Road, Hsin-Chu, 30010, Taiwan

Supporting Information

ABSTRACT: Unpredictable trends of charge mobility (μ) in multicyclic heteroarenes-contained polymers remain an obstacle in designing high performance polymers used in polymeric field effect transistors (PFETs). The roles of the comonomeric units in reaching high hole mobility (μ_h) of copolymers containing a heptacyclic arene unit, dithienocyclopentacarbazole (DTCC) were investigated in this study. A series of four DTCC-based alternating copolymers, **PDTCC-1T**, **PDTCC-3T**, **PDTCC-BDT**, and **PDTCC-TT**, were synthesized from the Pd-catalyzed copolymerizations between DTCC and comonomeric units including thiophene (1T), terthiophene (3T), benzodithiophene (BDT) and thienothiophene (TT) units. Among the four DTCC-based alternating copolymers, highest mobility of 1.36×10^{-2} cm^2 V^{-1} s^{-1} was reached in **PDTCC-3T**. Optoelectronic and 2D-WAXD studies revealed that strong electronic interaction and highly ordered solid-state structure were only observed in **PDTCC-3T**. It is attributed to the combination of two axisymmertric units, DTCC and 3T, linearized the polymer backbone, leading to a compact solid-state packing and high μ_h, while centrosymmertic comonomeric units, BDT and TT curved the polymer backbones of **PDTCC-BDT** and **PDTCC-TT**, which decreases solid-state order and μ_h. Furthermore, the short axisymmeritric 1T although results in a linear backbone of **PDTCC-1T**, comparing to 3T, it is too short to effectively reduce interchain steric hindrance caused by the solubilizing octyl chains on DTCC. Thus, effective $\pi-\pi$ stacking is hindered in **PDTCC-1T**, resulting in low μ_h. The macroscopic performances of μ_hs agreed well with the optoelectronic and 2D-WAXD studies. It is concluded that the linear backbone of DTCC copolymers is the prerequisite to reach ordered solid-state packing, which facilitate effective charge transport, and it depends on the prudent choose on the symmetry of the comonomeric unit. In addition, balance between the solubility and adequate crowdedness of lateral side chains is essential for a PFET material to be not only easily processed, but also effectively $\pi-\pi$ stack.

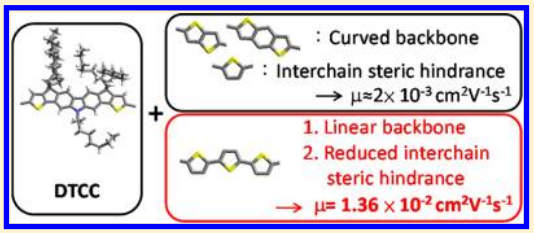

INTRODUCTION

Conjugated polymers have received significant scientific and industrial attentions in polymeric field-effect transistors (PFETs), because their solution-processability facilitates low-cost, large-scale productions, and the flexibility of polymers opens up the opportunities in producing flexible electronics.[1−6] The rigid and planar conjugated systems of ladder-type multicyclic heteroarenes are considered advantageous in facilitating better electron delocalization, suppressing interannular rotation, and reducing reorganization energy,[7−14] which are beneficial in reaching high intrinsic charge mobility (μ). μ over 1 cm^2 V^{-1} s^{-1} has been reported in copolymers containing multicyclic heteroarenes, such as naphtho[1,2-*b*:5,6-*b*′]-dithiophene,[15−17] dithieno[3,2-*b*;6,7-*b*]carbazole,[18] indacenodithiophene,[19,20] Triggered by these successes, considerable attentions have been drawn to further elongate the conjugation system of the ladder-type multicyclic heteroarenes.[7,21−28] Poly(2,7-carbazole) featured with deep-lying highest occupied molecular orbital energy levels (E_{HOMO}s) and moderate hole-transporting properties with hole mobilities (μ_hs) around $10^{-4}-10^{-3}$ cm^2 V^{-1} s^{-1}.[29] It is a useful core unit to make highly extended heteroarenes, since chemically rigidification of a central carbazole core with the two outer thiophenes of dithenylcarbazoles enables the effective synthesis of ladder-type heptacyclic arenes.[7,21−24] However, planarizing this conjugated system did not bring expected enhancements in μ. Instead, low μ_h was observed in the polymers containing the heptacyclic arenes, such as dithienocyclopentacarbazole (DTCC). The homopolymer of DTCC provided μ_h around 10^{-6} cm^2 V^{-1} s^{-1} and the values were below 3×10^{-4} cm^2 V^{-1} s^{-1} when DTCC copolymerized with other aromatic units.[21,22] In copolymers contained pentacyclic arenes such as silaindacenodithiophene,[30] dithieno[2,3-*b*;7,6-*b*]carbazole[18] and heptacyclic arenes, such as dithienopyrrolo-carbazole,[7] low mobility at the magnitude of 10^{-3} cm^2 V^{-1} s^{-1} was also reported. The inconstant and unpredictable trend of μ_h remains an obstacle to the design of high performance PFET materials.

In fact, while fusing neighboring aromatic systems effectively suppress the torsion and may promote better intermolecular π-stacking of the polymer backbones; it also stiffens the conjugated backbone and imposes much greater kinetic barrier to keep the conjugated units from their thermodynamically

Received: June 23, 2013
Revised: September 10, 2013
Published: September 24, 2013

Scheme 1. Chemical Structures of the DTCC Alternating Copolymers and the Linker Units

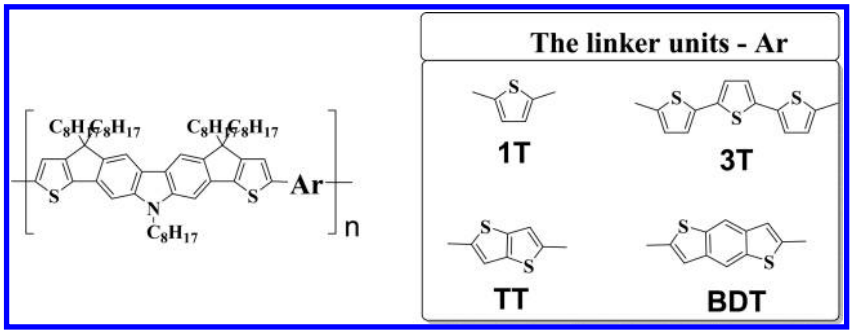

favorable ordered solid-state structure. Furthermore, the additional lateral aliphatic side chains introduced along with the bridge atoms also imposes steric hindrance for the π-stacking of the polymer backbones. The influences of these molecular variables on the performances of the conjugated polymers constructed with multicyclic arenes are important, but by far less studied. To this end, a series of conjugated alternating copolymers containing DTCC and linker units with varied length and rigidity as shown in Scheme 1 were synthesized. Their solid-state structures were characterized with two-dimensional (2D) wide X-ray diffractometer (WAXD) and their PFET performances were investigated and rationalized based on their solid-state characterizations. The study shows that although the ladder-type heptacyclic DTCC holds good planarity, their bulky lateral side chains prevent the close intermolecular packing. High mobility can be achieved only when a flexible linker unit with adequate length is adopted as the comonomeric unit to facilitate close intermolecular packing. Although rigid and fused linkers such as thienothopene (TT) and benzodithiophene (BDT) are general comonomeric units in many high performance PFET materials,[31−35] they actually curved and stiffened the conjugated backbone, which hindered intermolecular packing.

EXPERIMENTAL SECTION

General Measurement and Characterization. All chemicals were purchased from Aldrich, Acros or Luminescence and used as received unless otherwise specified. ^{1}H and ^{13}C NMR spectra were measured using a Varian 300 MHz instrument spectrometer. Fourier transform infrared (FTIR) spectra were on a Perkin-Elmer One Instrument by preparing KBr Pellets. Differential scanning calorimetery (DSC) was measured on a TA Q200 Instrument and thermogravimetric analysis (TGA) was recorded on a Perkin-Elmer Pyris under nitrogen atmosphere at a heating rate of 10 °C min^{-1} . Absorption spectra were collected on a HP8453 UV−vis spectrophotometer. The molecular weight of polymers were measured by the GPC method on a Viscotek VE2001GPC, and polystyrene was used as the standard (THF as the eluent). The electrochemical cyclic voltammetry (CV) was conducted on a CH Instruments Model 611D. A carbon glass coated with a thin polymer film was used as the working electrode and Ag/Ag$^+$ electrode as the reference electrode, while 0.1 M tetrabutylammoniumhexafluorophosphate (Bu_4NPF_6) in acetonitrile was the electrolyte. CV curves were calibrated using ferrocence as the standard, whose oxidation potential is set at −4.8 eV with respect to zero vacuum level. The E_{HOMO}s were derived from the equation $E_{HOMO} = -e(E_{ox}^{onset} - E_{(ferrocene)}^{onset} + 4.8)$ (eV). The E_{LUMO}s were derived from the equation $E_{LUMO} = -e\ (E_{red}^{onset} - E_{(ferrocene)}^{onset} + 4.8)$ (eV). For 2D WAXD patterns, Bruker APEX DUO single crystal diffraction was used and a INCOATEC 18 kW rotating I microfocus X-ray generator(Cu K_α radiation (0.1542 nm)) attached to an APEX II CCD camera was used. The exposure time to obtain high-quality patterns was 40 s. Computer molecular modeling was performed using the Cerius^2 package of Accelrys.

Materials. *Compound 2.* 2,7-Bis(4,4,5,5-tetramethyl-1,3,2-dioxaborolan-2-yl)-9-octyl-9H-carbazole (**1**)[36] (5 g, 9.41 mmol), ethyl 2-bromothiophene-3-carboxylate[37] (5.06 g, 21.6 mmol), K_2CO_3 (7,73 g, 56 mmol), Aliquant 336 (0.95 g, 2.4 mmol), and $Pd(PPh_3)_4$ (1.08 g, 0.94 mmol) were dissolved in deoxygenated toluene/H_2O (78 mL, 5:1, v/v). The reaction mixture was refluxed at 120 °C for 72 h and then extracted with diethyl ether (100 mL × 3) and water (150 mL). The collected organic layer was dried over $MgSO_4$. After removal of the solvent under reduced pressure, the residue was purified by column chromatography on silica gel (hexane/dichloromethane, v/v, 20/1) to give a yellow solid product **2** (4.5 g, 67%). ^{1}H NMR (300 MHz, $CDCl_3$): δ (ppm) 0.87 (t, J = 6.6 Hz, 3H), 1.4−1.0 (m, 16H), 2.0−1.8 (m, 2H), 4.20 (q, J = 7.1 Hz, 4H), 4.30 (t, J = 7.5 Hz, 2H), 7.28 (dd, J = 5.4 Hz, J = 0.9 Hz, 2H), 7.37 (d, J = 8.1 Hz, 2H), 7.55 (s, 2H), 7.56 (dd, J = 5.4 Hz, J = 0.9 Hz, 2H), 8.09 (d, J = 8.1 Hz, 2H).

Compound 3. To a solution of **2** (0.84 g, 1.43 mmol) in dry THF (20 mL) was added dropwise *n*-octyl magnesium bromide which was freshly prepared by reacting 1-bromooctane (2.21 g, 11.44 mmol) with magnesium turnings (0.313 g, 12.8 mmol). The reaction mixture was refluxed at 70 °C for 16 h and then quenched with water, followed by extraction with diethyl ether (50 mL × 3) and water (100 mL). The collected organic layer was dried over $MgSO_4$. After removal of the solvent under reduced pressure, the residue was purified by column chromatography on silica gel (hexane/ethyl acetate, v/v, 30/1) to give an orange sticky product **3** (0.54 g, 40%). ^{1}H NMR (300 MHz, $CDCl_3$): δ (ppm) 0.86 (m, 15H), 1.4−1.0 (m, 62H), 1.9−1.6 (m, 8H), 4.25 (t, J = 7.2 Hz, 2H), 7.01 (d, J = 5.4 Hz, 2H), 7.21 (d, J = 5.4 Hz, 2H), 7.28 (d, J = 8.1 Hz, 2H), 7.43 (s, 2H), 8.06 (d, J = 8.1 Hz, 2H).

DTCC. To a solution of **3** (0.47 g, 0.49 mmol) in dichloromethane (30 mL) was added boron trifluoridediethyl etherate (1.5 mL). The reaction mixture was stirred for 10 h at room temperature and then was extracted with dichloromethane (50 mL × 4) and water (100 mL). The collected organic layer was dried over $MgSO_4$. After removal of the solvent under reduced pressure, the residue was purified by column chromatography on silica gel (hexane) to give **DTCC** as a yellow solid (0.22 g, 50%). ^{1}H NMR (300 MHz, $CDCl_3$): δ (ppm) 0.9−0.7 (m, 25H), 1.4−1.0 (m, 50H), 2.0−1.8 (m, 8 H), 4.31 (t, J = 7.2 Hz, 2H), 6.99 (d, J = 8.1 Hz, 2H), 7.28 (d, J = 8.1 Hz, 2H), 7.34 (s, 2H), 7.90 (s, 2H).

DTCC-Br. *N*-Bromosuccimide (0.097 g, 0.546 mmol) was added in one portion to a solution of ***DTCC*** (0.24 g, 0.26 mmol) in THF (60 mL). The reaction was stirred under darkness for 12 h at room temperature. The mixture solution was extracted with diethyl ether (60 mL × 3) and water (60 mL). The combined organic layer was dried over $MgSO_4$. After removal of the solvent under reduced pressure, the residue was purified by column chromatography on silica gel (hexane) to give ***DTCC-Br*** as a yellow solid (0.251 g, 90%). ^{1}H NMR (300 MHz, $CDCl_3$): δ (ppm) 1.0−0.7 (m, 25H), 1.3−1.0 (m, 50H), 2.1−1.9 (m, 8H), 4.28 (t, 2H), 7.00 (s, 2H), 7.26 (s, 2H), 7.87 (s, 2H).

General Procedure for the Copolymerization Reaction. **DTCC-Br**, comonomer (1.0 equiv per DTCC-Br), tris(dibenzylideneacetone) dipalladium (0.05 equiv per **DTCC-Br**), tris(2-methylphenyl)phosphine (0.4 equiv per DTCC-Br), and a

dx.doi.org/10.1021/ma4012973 | *Macromolecules* 2013, 46, 7687−7695

Scheme 2. Synthetic Route of DTCC-Br

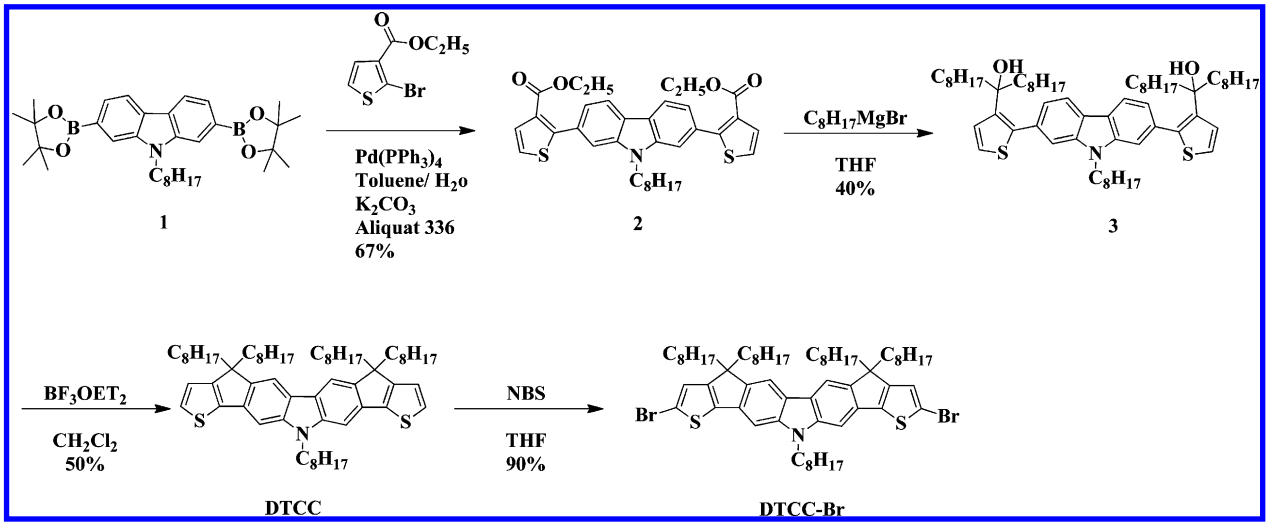

Scheme 3. Synthetic Route of the Alternating Copolymers

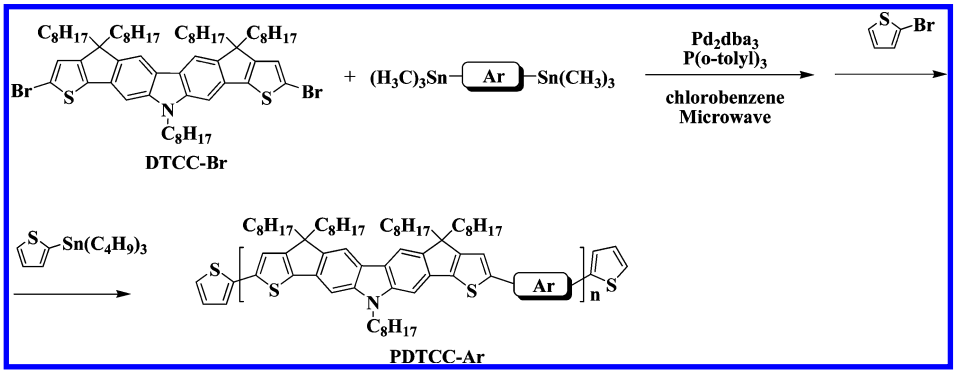

minimum amount of deoxygenated chlorobenzene to full dissolve the monomers were introduced to a 25 mL round-bottom flask. The mixture was then degassed by bubbling nitrogen for 10 min at room temperature. The round-bottom flask was placed into the microwave reactor and reacted at 180 °C for 50 min under 270 W. Then, 2-bromothiophene (1.0 eq. per DTCC-Br) was added to the mixture solution and reacted for 10 min under 270 W. Finally, tributyl-(thiophen-2-yl)stannane (2 eq. per DTCC-Br) was added to the mixture solution and reacted for 10 min under 270 W. The solution was added into methanol dropwise. The precipitate was collected by filtration and washed by Soxhlet extraction with acetone for 24 h and hexane for 24 h sequentially. The product was redissolved in THF. The Pd-thiol gel (Silicycle Inc.) (0.02 eq. per DTCC-Br) was added to above THF solution to remove the residual Pd catalyst. After filtration and removal of the solvent, the polymer was redissolved in THF again and added into methanol to reprecipitate. The purified polymer was collected by filtration and dried under vacuum for 1 day.

PDTCC-1T. Following the general procedure for polymer synthesis, **DTCC-Br** (0.1 g, 0.0931 mmol), 2,5-bis(trimethylstannyl)thiophene (38.14 mg, 0.0931 mmol), tris(dibenzylideneacetone) dipalladium (4.12 mg, 0.0045 mmol), tris(2-methylphenyl)phosphine (10.94 mg, 0.036 mmol), deoxygenated chlorobenzene (4 mL), 2-bromothiophene (0.15 g, 0.931 mmol), tributyl(thiophen-2-yl)stannane (0.7 g, 1.86 mmol), and Pd-thiol gel (Silicycle Inc.) (15 mg, 0.018 mmol) were used. **PDTCC-1T** was obtained as a red solid (38 mg). Yield: 40%, M_n = 67.8 kDa, PDI = 2.18. ^{1}H NMR (400 MHz, THF-d_8): δ (ppm) 0.80–0.88 (m, 15H), 1.15–1.28 (m, 60H), 2.03–2.13 (m, 8H), 4.46 (br, 2H), 6.25 (br, 2H), 7.09 (br, 2H), 7.51 (br, 2H), 8.02 (br, 2H).

PDTCC-3T. **DTCC-Br** (100 mg, 0.093 mmol), 5,5″-bis-(trimethylstannyl)-2,2′:5′,2″-terthiophene (53.60 mg, 0.093 mmol), tris(dibenzylideneacetone) dipalladium (4.575 mg, 0.005 mmol), tris(2-methylphenyl)phosphine (12.12 mg, 0.04 mmol), deoxygenated chlorobenzene (4 mL), 2-bromothiophene (0.15 g, 0.93 mmol), tributyl(thiophen-2-yl)stannane (0.7 g, 1.86 mmol), and Pd-thiol gel (Silicycle Inc.) (17 mg, 0.02 mmol) were used. **PDTCC-3T** was obtained as a red solid (99 mg). Yield: 91%, M_n = 15.2 kDa, PDI = 2.85. ^{1}H NMR (400 MHz, THF-d_8): δ (ppm) 0.80–0.88 (m, 15H), 1.16–1.29 (m, 60H), 2.05–2.13 (m, 8H), 4.41 (br, 2H), 6.27 (br, 2H), 7.03 (br, 2H), 7.21 (br, 2H), 7.27 (br, 2H), 7.49 (br, 2H), 8.01 (br, 2H).

PDTCC-TT. **DTCC-Br** (150 mg, 0.139 mmol), 2,5-bis-(trimethylstannyl)thieno[3,2-b]thiophene (65.041 mg, 0.139 mmol), tris(dibenzylideneacetone) dipalladium (6.391 mg, 0.007 mmol), tris(2-methylphenyl)phosphine (17 mg, 0.06 mmol), deoxygenated chlorobenzene (4 mL), 2-bromothiophene (0.23 g, 1.4 mmol), tributyl(thiophen-2-yl)stannane (1.05 g, 2.8 mmol), and Pd-thiol gel (Silicycle Inc.) (23.7 mg, 0.028 mmol) were used. **PDTCC-TT** was obtained as a red solid (105 mg). Yield: 71%, M_n = 47.9 kDa, PDI = 1.48. ^{1}H NMR (400 MHz, THF-d_8): δ (ppm) 0.75–0.88 (m, 15H), 1.14–1.28 (m, 60H), 2.02–2.04 (m, 8H), 4.41 (br, 2H), 6.25 (br, 2H), 6.95 (br, 2H), 7.52 (br, 2H), 8.01 (br, 2H).

PDTCC-BDT. **DTCC-Br** (110 mg, 0.1024 mmol), 2,6-bis-(trimethylstannyl)benzo[1,2-b:4,5-b′]dithiophene (52.82 mg, 0.1024 mmol), tris(dibenzylideneacetone) dipalladium (4.68 mg, 0.0051 mmol), tris(2-methylphenyl)phosphine (12.46 mg, 0.041 mmol), deoxygenated chlorobenzene (4 mL), 2-bromothiophene (0.16 g, 1.024 mmol), tributyl(thiophen-2-yl)stannane (0.76 g, 2.05 mmol), and Pd-thiol gel (Silicycle Inc.) (17 mg, 0.02 mmol) were used. **PDTCC-BDT** was obtained as a red solid (105 mg). Yield: 93%, M_n = 23.2 kDa, PDI = 3.08. ^{1}H NMR (400 MHz, THF-d_8): δ (ppm) 076–0.87 (m, 15H), 1.14–1.32 (m, 60H), 2.07–2.18 (m, 8H), 4.41 (br,

dx.doi.org/10.1021/ma4012973 | Macromolecules 2013, 46, 7687–7695

2H), 6.31 (br, 2H), 6.88 (br, 2H), 7.40 (br, 2H), 7.57 (br, 2H), 8.10 (br, 2H).

OFET Fabrication. An n-type heavily doped Si wafer with a SiO_2 layer of 300 nm and a capacitance per unit area of 11 nF cm^{-2} was used as the gate electrode and dielectric layer. Thin films (40−60 nm in thickness) of polymers were deposited on octadecyltrichlorosilane (ODTS)-treated SiO_2/Si substrates by spin-coating their *o*-dichlorobenzene solutions (5 mg mL^{-1}). Then, the thin films were annealed at different temperature (120, or 200 °C) for 10 min. Gold source and drain electrodes (30 nm in thickness) were deposited by vacuum evaporation on the organic layer through a shadow mask, affording a bottom-gate, top-contact device configuration. Electrical measurements of OTFT devices were carried out at room temperature in air using a 4156C, Agilent Technologies. The field-effect mobility was calculated in the saturation regime by using the equation $I_{DS} = (\mu WC_i/2L)(V_G - V_T)^2$, where I_{DS} is the drain-source current, μ is the field-effect mobility, W is the channel width (500 μm), L is the channel length (50 μm), C_i is the capacitance per unit area of the gate dielectric layer, and V_G is the gate voltage.

RESULTS AND DISCUSSION

Synthesis of the DTCC Monomer and Copolymers. The synthetic routes toward the monomers and the copolymers are depicted in Scheme 2 and Scheme 3. 9-Octyl-2,7-bis(4,4,5,5-tetramethyl-1,3,2-dioxaborolan-2-yl)-9*H*-carbazole **1** was reacted with ethyl 2-bromothiophene-3-carboxylate by Suzuki coupling to obtain compound **2**. Grignard reaction was applied to attach the octyl chains onto **2** and resulted in compound **3**. Intramolecular cyclization of **3** catalyzed by boron trifluoride etherate afforded **DTCC** in 50% yield. Monomer **DTCC-Br** was obtained in 90% yield by bromination of **DTCC** with N-bromosuccimide (NBS) in tetrahydrofuran (THF). The obtained monomer **DTCC-Br** was then copolymerized with 2,5-bis(trimethylstannyl)thiophene, 5,5″-bis(trimethylstannyl)-2,2′:5′,2″- terthiophene, 2,5-bis(trimethylstannyl)thieno[3,2-b]thiophene, and 2,6-bis(trimethylstannyl)benzo[1,2-b:4,5-b′]-dithiophene under Stille coupling conditions to give the alternating copolymers **PDTCC-1T**, **PDTCC-3T**, **PDTCC-TT**, and **PDTCC-BDT**. The number-average molecular weights (M_n) and polydispersity (PDI) of the copolymers were evaluated by gel permeation chromatography (GPC) in THF summarized in Table 1. The M_n of the copolymers are between 15 to 68 kDa and the PDI are between 1.5 to 3.1.

Table 1. Molecular Weights and Polydispersity of the DTCC Copolymers

copolymer	M_n (kDa)	M_w (kDa)	PDI (M_w/M_n)
PDTCC-1T	68	148	2.2
PDTCC-3T	15	43	2.9
PDTCC-BDT	23	72	3.1
PDTCC-TT	48	71	1.5

Thermal Properties of the DTCC Copolymers. The thermal stabilities of the copolymers were studied by thermogravimetric analysis (TGA). All copolymers exhibited 5% weight loss temperature (T_d) above 380 °C as shown in Figure S1, indicating the good thermal stability of the copolymers. No observable phase transition was shown in the differential scanning calorimetry (DSC) measurements of all copolymers in the temperature range between 0−270 °C (Figure S2). Two-dimensional (2D) wide-angle X-ray diffraction (WAXD) study (vide infra) suggests that the copolymers possess liquid crystalline (LC) order at room temperature. The LC phases of the copolymers thus have isotropization temperature (T_i) above 270 °C.

Optical and Electrochemical Properties of the DTCC Copolymers. The solution and thin-film UV−vis absorption spectra of all copolymers are shown in Figure 1 and the relevant data were summarized in Table 2. In the toluene solution, **PDTCC-1T**, **PDTCC-3T**, and **PDTCC-TT** have similar λ_{max}s for their absorption bands, suggesting that except for BDT, the linker units-1T, 3T and TT, show little influence on the relative positions of their frontier orbitals. More clearly vibronic structures were observed for **PDTCC-1T**, **PDTCC-TT**, and **PDTCC-BDT**, indicating that the conjugated systems in **PDTCC-1T**, **PDTCC-TT**, and **PDTCC-BDT** have higher rigidity than **PDTCC-3T**. Thus, it is likely that two additional interannular single bonds incorporated along with the 3T units impose better flexibility to the conjugated backbones. Compared to the solution absorption, only **PDTCC-3T** shows obvious absorption shifts in its thin-film absorption. Thus, no strong intermolecular electronic interactions are present among the conjugated backbones in the thin films of **PDTCC-1T**, **PDTCC-TT**, and **PDTCC-BDT**.[37,38] It can be attributed to the great steric hindrance imparted by the peripheral octyl side chains on the DTCC unit as illustrated in Figure 2a, which prevents the close stacking and strong intermolecular electronic interactions. On the contrary, evident broadening of the **PDTCC-3T** absorption implied strong intermolecular electronic interactions in the solid state. Observation of both hypsochromic and bathochromic shifts indicating the coexistence of H- and J-aggregations of the conjugated systems. Therefore, the photophysical results of the copolymers indicate that 3T is a more flexible linker than the short or fused 1T, TT, and BDT units. Its elongated structure also promotes better intermolecular stacking and stronger electronic interactions for the copolymer constructed with steric hindered multicyclic arenes. Interesting, the effect was not observed in the rigid extended linker, i.e., TT and BDT. Molecular modeling of the conjugated backbones of **PDTCC-1T**, **PDTCC-3T**, **PDTCC-BDT**, and **PDTCC-TT** are shown in Figure 2b−e. **PDTCC-3T** has a linear backbone at its most stable conformation. On the other hand, due to the linear geometry of BDT and TT, **PDTCC-BDT** and **PDTCC-TT** actually have curved backbones as illustrated in Figure 2, parts d and e. The curved backbones are thus difficult to stack and the strong intermolecular electronic interactions are prevented.

Cyclic voltammetry (CV) was used to estimate the energy levels of the highest occupied molecular orbitals (E_{HOMO}s) and the lowest unoccupied molecular orbital (E_{LUMO}s) of the copolymers. The electrochemical properties were also summarized in Table 2. The corresponding electrochemical band gaps (E_g^{elec}) of four copolymers have no significant differences, revealing again that linker units have trivial effect on the frontier orbitals.

Solid-State Structures of the DTCC Copolymers. 2D WAXD was applied to gain insights into the solid-state structures, and the structure−property relationships of the DTCC copolymers. Figure 3 shows the 2D WAXD patterns of the DTCC copolymers. The samples were sheared at temperatures between 250 and 310 °C, cooled to room temperature, and used in the following 2D WAXD measurements. Intriguingly, diffraction arcs were observed in **PDTCC-1T** and **PDTCC-3T**, but only diffraction rings were observed in **PDTCC-TT** and **PDTCC-BDT**. It indicates that oriented ordered domains can be induced via the shearing process in

dx.doi.org/10.1021/ma4012973 | *Macromolecules* 2013, 46, 7687−7695

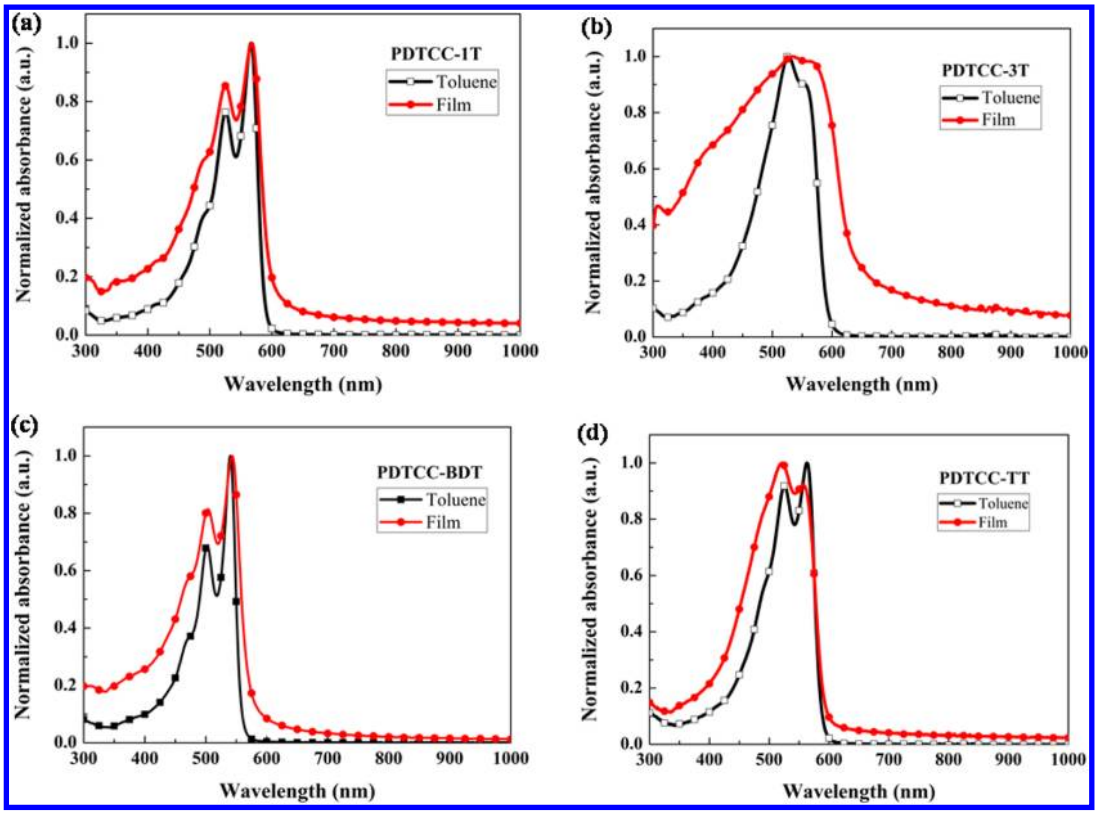

Figure 1. Normalized solution and thin film absorption spectra of (a) **PDTCC-1T**, (b) **PDTCC-3T**, (c) **PDTCC-BDT**, and (d) **PDTCC-TT**.

Table 2. Photophysical Properties and Electrochemical Data of the Copolymers

copolymer	solution λ_{max} (nm)	thin-film λ_{max} (nm)	E_g^{opt} (eV)[a]	E_{HOMO} (eV)	E_{LUMO} (eV)	E_g^{elec} (eV)[b]
PDTCC-1T	526, 566	526, 568	2.1	−5.1	−2.5	2.6
PDTCC-3T	526, 554	534, 565	1.9	−5.1	−2.7	2.5
PDTCC-TT	525, 563	521, 555	2.1	−5.2	−2.6	2.6
PDTCC-BDT	502, 540	504, 543	2.2	−5.1	−2.7	2.4

[a] E_g^{opt} from the onset of UV spectra in thin film. [b] $E_g^{elec} = |E_{HOMO} - E_{LUMO}|$

PDTCC-1T and **PDTCC-3T**, but not in **PDTCC-TT** and **PDTCC-BDT**. 3T, TT and BDT are more extended conjugated linkers than 1T. 3T is the most extended one, but it is not fused multicyclic arenes like TT and BDT. The hardship in orienting **PDTCC-TT** and **PDTCC-BDT** thus implies that fused conjugated linkers stiffen the conjugated backbones and make them more difficult to be oriented with shearing. This agrees with the conclusion from the UV−vis absorption results.

In the low-angle region, diffraction rings with *d*-spacing of 2.27 nm were found in both **PDTCC-TT** and **PDTCC-BDT** (Figure 3c and 3d). The diffraction arcs with *d*-spacing of 1.42 nm for **PDTCC-1T**, and *d*-spacing of 1.62 nm for **PDTCC-3T** were located at the equator (Figure 3a and 3b). The *d*-spacings fit with the lateral dimensions of the copolymers illustrated in Figure 2b-2e, and therefore represent the ordered lamellar structures along the lateral direction of copolymer chains as illustrated in Figure 4a−c and Figure S4. The octyl chains have certain degree of interdigitation, since the *d*-spacings of the lamellar structures are smaller than the lateral dimensions of copolymers with extended octyl chains. The absence of higher-order peaks suggested that the lamellar arrangement is at most with quasi-long-range order. The much larger interchain distance of **PDTCC-TT** and **PDTCC-BDT** in the lamellar structure concurs with the results in the molecular modeling showing that their conjugated backbone are more curved and difficult to be packed closely, as illustrated in Figure 4c. Along the meridian direction, the diffraction arc with *d*-spacing of 0.49 nm in **PDTCC-1T**, and 0.45 nm in **PDTCC-3T** represent the average distance among the aromatic units along the chain direction. The observation also supports that the chain direction of **PDTCC-1T** and **PDTCC-3T** is aligned with the shearing direction.

At high-angle region on the equator, another pair of diffraction arcs with *d*-spacing of 0.37 nm was also observed in **PDTCC-3T**, which indicates the presence of periodically $\pi-\pi$ stacking with intermolecular distance of 0.37 nm, as illustrated in Figure 4e. On the contrary, a more diffused scattering halo with *d*-spacing of 0.37 nm was shown in **PDTCC-1T** (Figure 3a), and no observable diffraction for the ordered $\pi-\pi$ stacking were found in **PDTCC-TT** and **PDTCC-BDT**. Thus, the curved backbone of **PDTCC-TT** and **PDTCC-BDT** not only hindered compact lamellar arrangements, but also prevents ordered $\pi-\pi$ stacking in the solid state of the copolymers. The result also consists with the weak electronic interactions observed from the UV−vis absorption measurements. Although like **PDTCC-3T**, the backbone of **PDTCC-1T** is close to straight, only weak scattering halo for $\pi-\pi$ stacking and weak electronic interaction present in its solid state. This is attributed to the crowdedness of the lateral alkyl chains, which curbs the ordered $\pi-\pi$ stacking, as illustrated in Figure 4d. On the other hand, the

dx.doi.org/10.1021/ma4012973 | *Macromolecules* 2013, 46, 7687−7695

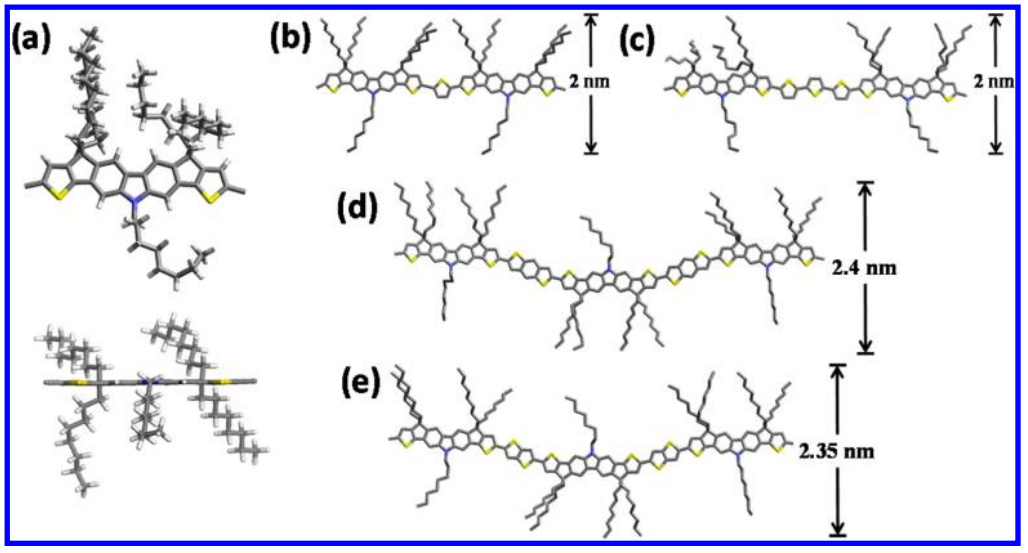

Figure 2. (a) Top view and side view of energy-minimized molecular models of a DTCC unit. Molecular models of the conjugated backbones of (b) **PDTCC-1T**, (c) **PDTCC-3T**, (d) **PDTCC-BDT**, and (e) **PDTCC-TT**. The hydrogen atoms were omitted in parts b–e for clarity.

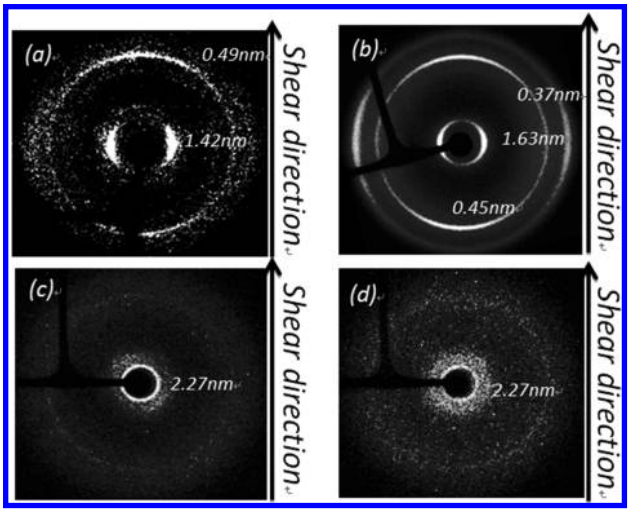

Figure 3. 2D WAXD patterns of the ordered phases of (a) **PDTCC-1T**, (b) **PDTCC-3T**, (c) **PDTCC-BDT**, and (d) **PDTCC-TT** after shearing. Solid arrow indicates the direction of mechanical shearing force applied on the sample. The incident X-ray beam was along the normal direction of the 2D patterns.

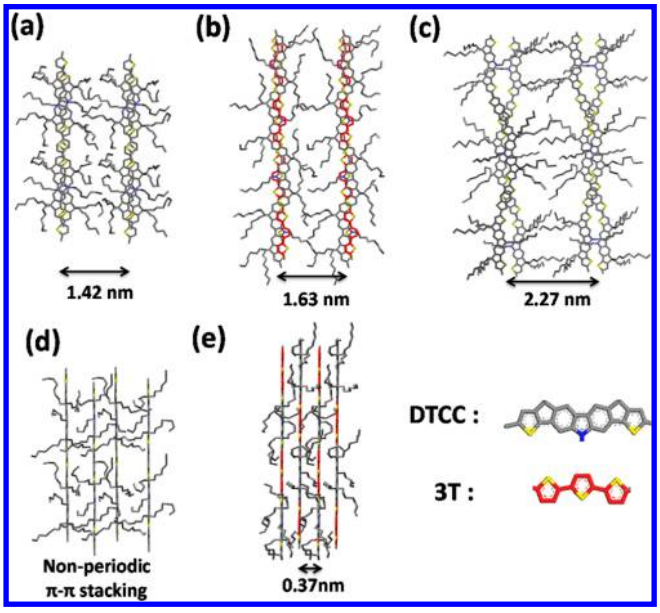

Figure 4. Schematic illustrations of the lamellar structures of (a) **PDTCC-1T**, (b) **PDTCC-3T** and (c) **PDTCC-BDT**. Illustrations of the $\pi-\pi$ stacking of a set of four conjugated chains of (d) **PDTCC-1T** and (e) **PDTCC-3T**.

longer linker -3T provides more space to accommodate the five octyl groups on the DTCC units, and facilitate close and ordered $\pi-\pi$ stacking. This is also supported by the larger *d*-spacing of 1.63 nm for the lamellar structure of **PDTCC-3T** than that of 1.42 nm in **PDTCC-1T**, because more effective $\pi-\pi$ stacking should result in the higher degree of lateral extension for the octyl side chains and therefore larger lamellar distance.

Polymer Field-Effect Transistor Performances of the DTCC Copolymers. In order to investigate the charge transport properties of the copolymers, bottom-gate top contact PFETs were fabricated with evaporated gold source/drain electrodes and octadecyltrichlorosilane-modified SiO_2 gate dielectric on n-doped silicon wafer surface. The copolymer thin film was prepared by spin-coating a 5 mg/mL *o*-dichlorobenzene copolymer solution onto a SiO_2/Si substrate, and annealed at 120 °C for 10 min under nitrogen. The transfer and output characteristics are shown in Figure 5, and the device performances were summarized in Table 3. The μ_hs were obtained from the transfer characteristics of the devices in saturation regime. The highest μ_h of 1.4×10^{-2} cm^2 V^{-1} s^{-1} with an on–off ratio of 8×10^4 was provided by **PDTCC-3T**, whereas **PDTCC-1T**, **PDTCC-BDT**, and **PDTCC-TT** show about an order of magnitude lower μ_h of $(1.4–2.4) \times 10^{-3}$ cm^2 V^{-1} s^{-1} with on–off ratios between $0.8–8 \times 10^4$. Since **PDTCC-3T** possesses the most ordered solid-state structure and strongest intermolecular electronic interaction as indicated from the 2D WAXD patterns and UV–vis spectra, it is evident that the solid-state order plays an essential role in the PFET performances of the copolymers. The compact lamellar structure and ordered $\pi-\pi$ stacking of **PDTCC-3T** enables effective intermolecular electronic interaction and consequently resulted in the highest μ_h among the DTCC based-copolymers.

dx.doi.org/10.1021/ma4012973 | *Macromolecules* 2013, 46, 7687–7695

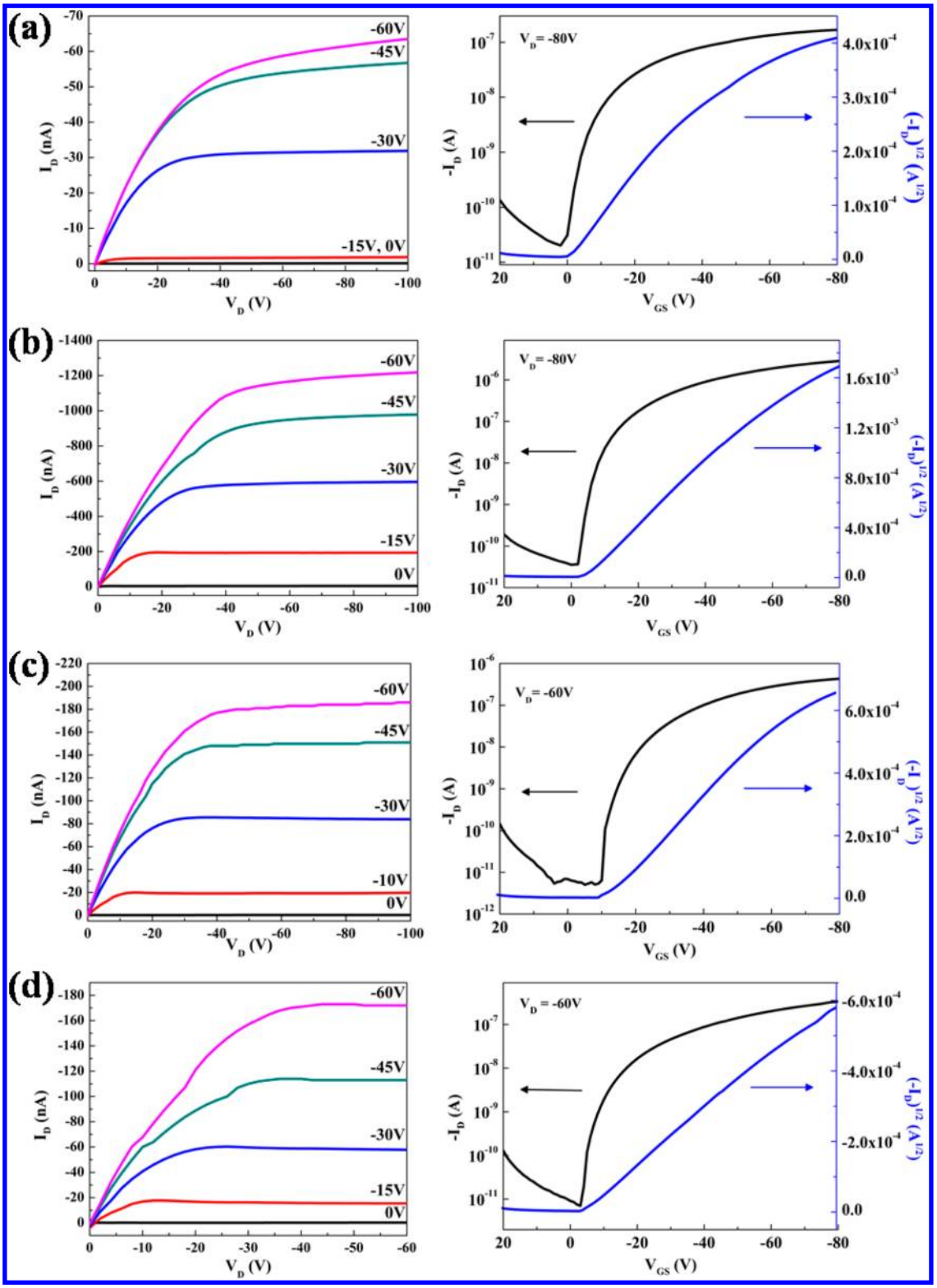

Figure 5. Transfer (right) and output (right) characterustices of the PFET devices of (a) **PDTCC-1T**, (b) **PDTCC-3T**, (c) **PDTCC-BDT**, and (d) **PDTCC-TT**.

The role of the linker units in the performances of donor–acceptor based low bandgap (LBG) copolymers was previously demonstrated by Pei et al. in isoindigo-based polymers.[32] Their study showed that centrosymmetric linkers lead to the straighter backbones which are more favorable in forming ordered solid-state structures than the wavy backbones formed by the axisymmetric ones. Interestingly, in the copolymer system containing heptacyclic arenes, the axial symmetrical linears, i.e. 1T and 3T, actually allow the formation of more ordered solid-state structures. The seeming contradiction is understandable, since the isodingo unit is a centrosymmetrical, but the DTCC unit in this study is axial symmetrical. Our

dx.doi.org/10.1021/ma4012973 | *Macromolecules* 2013, 46, 7687–7695

Table 3. The field effect transistors characteristics of PDTCC-1T, PDTCC-3T, PDTCC-BDT and PDTCC-TT

copolymers	highest μ_h (average μ_h)[a] ($cm^2\ V^{-1}\ s^{-1}$)	$I_{on/off}$	V_T (V)
PDTCC-1T	1.8×10^{-3} (1.2×10^{-3})	8×10^3	0.8
PDTCC-3T	1.4×10^{-2} (9.4×10^{-3})	8×10^4	−4.6
PDTCC-BDT	2.4×10^{-3} (2.1×10^{-3})	8×10^4	−13.3
PDTCC-TT	1.4×10^{-3} (1.0×10^{-3})	4×10^4	−3

[a]Average value of over three devices.

molecular modeling suggested that linear backbone can be achieved in an alternating copolymer system where either both comonomer units are centrosymmetrical or both are axial symmetrical. On the other hand, combining a centrosymmetrical unit with an axial symmetrical one curves the conjugated backbone, and may curb the solid-state order and device efficiency. Furthermore, since the lamellar structure of conjugated polymers generally represents the nanophase separation between the flexible lateral side chains and the rigid conjugated backbones, the crowdedness of the alkyl side chains has to be well-adjusted to avoid hindering the effective $\pi-\pi$ stacking. In other words, a delicate balance between the solubility of the polymer and the crowdedness of the lateral side chains is essential in order to obtain material, which is not only easily processed, but also highly ordered in the solid state. Müllen and co-workers presented the importance of the balance between solubility and solid-state order from another aspect.[33,39] In their system of benzodithiophene- (BDT-) containing polymers, the highest transistor performance was delivered from a BDT copolymer with a slightly curved backbone rather than the one with a linear backbone. Despite the linear analogue is advantageous with close intermolecular distance, the inferior performance was attributed to its poor solubility, which hindered the forming of uniform active layer and limited the device from reaching higher mobilities.[33]

CONCLUSION

Although it is generally considered that better electron delocalization, less interannular rotation and reorganization energy of ladder-type multicyclic heteroarenes are beneficial to reach high μ in PFET, the unpredictable trend in the μ_hs of multicyclic heteroarenes containing copolymers remains an obstacle to design high performance PFET materials. This study shows the importance of comonomeric units to the structures and performances of alternating copolymers containing a heptacyclic arene unit DTCC. Optoelectronic and 2D-WAXD studies revealed that stronger electronic interaction and well-ordered solid-state structure were only observed in the copolymer with 3T, which was one of the four comonomeric units (1T, 3T, BDT and TT) studied. The combination of the axisymmertric DTCC with the centrosymmertic units TT and BDT respectively curved the polymer backbones, and prevented compact and highly ordered solid-state structures of **PDTCC-BDT** and **PDTCC-TT**. Consequently, the copolymers showed low μ_hs around 2×10^{-3} $cm^2\ V^{-1}\ s^{-1}$. The axisymmertric comonomeric units 1T and 3T allowed the polymer backbones to adopt linearity conformations; therefore **PDTCC-1T** and **PDTCC-3T** resulted in better solid-state orders. However, the short 1T unit was insufficient in reducing the interchain steric hindrance caused by the solubilizing octyl groups on the DTCC units. Thus, effective $\pi-\pi$ stacking and good μ_h were not achieved by **PDTCC-1T**. On the other hand, **PDTCC-3T** had the highest μ_h of 1.36×10^{-2} $cm^2\ V^{-1}\ s^{-1}$ among the copolymers because the comonomeric unit 3T facilitated the formation of linear backbone, and provided sufficiently spaces to accommodate octyl side chains. As a result, **PDTCC-3T** which possessed high solid-state order with compact $\pi-\pi$ stacking and strong intermolecular electronic interactions as indicated by the 2D-WAXD pattern and UV−vis absorption spectrum obtained the highest μ_h.

ASSOCIATED CONTENT

Supporting Information

TGA and DSC thermograms, cyclic voltammograms, and synthesis and characterizations details. This material is available free of charge via the Internet at http://pubs.acs.org.

AUTHOR INFORMATION

Corresponding Authors

*E-mail: kclwang@nctu.edu.tw (C.-L.W.).
*E-mail: cshsu@mail.nctu.edu.tw (C.-S.H.).

Notes

The authors declare no competing financial interest.

ACKNOWLEDGMENTS

This work is supported by the National Science Council and "Aiming for the Top University Program" of the National Chiao Tung University and Ministry of Education, Taiwan, R.O.C.

REFERENCES

(1) Sirringhaus, H.; Tessler, N.; Friend, R. H. *Science* **1998**, *280*, 1741−1744.
(2) Cicoira, F.; Santato, C. *Adv. Funct. Mater.* **2007**, *17*, 3421−3434.
(3) Sirringhaus, H. *Adv. Mater.* **2005**, *17*, 2411−2425.
(4) Ling, M. M.; Bao, Z. *Chem. Mater.* **2004**, *16*, 4824−4840.
(5) Salleo, A. *Mater. Today* **2007**, *10*, 38−45.
(6) Arias, A. C.; Ready, S. E.; Lujan, R.; Wong, W. S.; Paul, K. E.; Salleo, A.; Chabinyc, M. L.; Apte, R.; Street, R. A.; Wu, Y.; Liu, P.; Ong, B. *Appl. Phys. Lett.* **2004**, *85*, 3304−3306.
(7) Wu, J.-S.; Cheng, Y.-J.; Lin, T.-Y.; Chang, C.-Y.; Shih, P.-I.; Hsu, C.-S. *Adv. Funct. Mater.* **2012**, *22*, 1711−1722.
(8) Mas-Torrent, M.; Rovira, C. *Chem. Rev.* **2011**, *111*, 4833−4856.
(9) Malagoli, M.; Brédas, J. L. *Chem. Phys. Lett.* **2000**, *327*, 13−17.
(10) Marcus, R. A. *Rev. Mod. Phys.* **1993**, *65*, 599−610.
(11) Brédas, J. L.; Calbert, J. P.; da Silva Filho, D. A.; Cornil, J. *Proc. Natl. Acad. Sci. U.S.A.* **2002**, *99*, 5804−5809.
(12) Baek, N. S.; Hau, S. K.; Yip, H.-L.; Acton, O.; Chen, K.-S.; Jen, A. K. Y. *Chem. Mater.* **2008**, *20*, 5734−5736.
(13) Osaka, I.; Abe, T.; Shinamura, S.; Takimiya, K. *J. Am. Chem. Soc.* **2011**, *133*, 6852−6860.
(14) Liang, Y.; Wu, Y.; Feng, D.; Tsai, S.-T.; Son, H.-J.; Li, G.; Yu, L. *J. Am. Chem. Soc.* **2008**, *131*, 56−57.
(15) Osaka, I.; Abe, T.; Shimawaki, M.; Koganezawa, T.; Takimiya, K. *ACS Macro Lett.* **2012**, *1*, 437−440.
(16) Osaka, I.; Abe, T.; Shinamura, S.; Miyazaki, E.; Takimiya, K. *J. Am. Chem. Soc.* **2010**, *132*, 5000−5001.
(17) Takimiya, K.; Osaka, I.; Shinamura, S.; Miyazaki, E. *Proc. SPIE* **2011**, 811702−811702.
(18) Deng, Y.; Chen, Y.; Zhang, X.; Tian, H.; Bao, C.; Yan, D.; Geng, Y.; Wang, F. *Macromolecules* **2012**, *45*, 8621−8627.
(19) Zhang, W.; Smith, J.; Watkins, S. E.; Gysel, R.; McGehee, M.; Salleo, A.; Kirkpatrick, J.; Ashraf, S.; Anthopoulos, T.; Heeney, M.; McCulloch, I. *J. Am. Chem. Soc.* **2010**, *132*, 11437−11439.

(20) Bronstein, H.; Leem, D. S.; Hamilton, R.; Woebkenberg, P.; King, S.; Zhang, W.; Ashraf, R. S.; Heeney, M.; Anthopoulos, T. D.; Mello, J. d.; McCulloch, I. *Macromolecules* **2011**, *44*, 6649−6652.
(21) Cheedarala, R. K.; Kim, G.-H.; Cho, S.; Lee, J.; Kim, J.; Song, H.-K.; Kim, J. Y.; Yang, C. *J. Mater. Chem.* **2011**, *21*, 843−850.
(22) Zheng, Q.; Chen, S.; Zhang, B.; Wang, L.; Tang, C.; Katz, H. E. *Org. Lett.* **2010**, *13*, 324−327.
(23) Wu, J.-S.; Cheng, Y.-J.; Dubosc, M.; Hsieh, C.-H.; Chang, C.-Y.; Hsu, C.-S. *Chem. Commun.* **2010**, *46*, 3259−3261.
(24) Cheng, Y.-J.; Wu, J.-S.; Shih, P.-I.; Chang, C.-Y.; Jwo, P.-C.; Kao, W.-S.; Hsu, C.-S. *Chem. Mater.* **2011**, *23*, 2361−2369.
(25) Xu, Y.-X.; Chueh, C.-C.; Yip, H.-L.; Ding, F.-Z.; Li, Y.-X.; Li, C.-Z.; Li, X.; Chen, W.-C.; Jen, A. K. Y. *Adv. Mater.* **2012**, *24*, 6356−6361.
(26) Bronstein, H.; Ashraf, R. S.; Kim, Y.; White, A. J. P.; Anthopoulos, T.; Song, K.; James, D.; Zhang, W.; McCulloch, I. *Macromol. Rapid Commun.* **2011**, *32*, 1664−1668.
(27) Biniek, L.; Schroeder, B. C.; Donaghey, J. E.; Yaacobi-Gross, N.; Ashraf, R. S.; Soon, Y. W.; Nielsen, C. B.; Durrant, J. R.; Anthopoulos, T. D.; McCulloch, I. *Macromolecules* **2013**, *46*, 727−735.
(28) Wu, J.-S.; Lin, C.-T.; Wang, C.-L.; Cheng, Y.-J.; Hsu, C.-S. *Chem. Mater.* **2012**, *24*, 2391−2399.
(29) Blouin, N.; Leclerc, M. *Acc. Chem. Res.* **2008**, *41*, 1110−1119.
(30) Schroeder, B. C.; Huang, Z.; Ashraf, R. S.; Smith, J.; D'Angelo, P.; Watkins, S. E.; Anthopoulos, T. D.; Durrant, J. R.; McCulloch, I. *Adv. Funct. Mater.* **2012**, *22*, 1663−1670.
(31) Nielsen, C. B.; Turbiez, M.; McCulloch, I. *Adv. Mater.* **2013**, *25*, 1859−1880.
(32) Lei, T.; Cao, Y.; Zhou, X.; Peng, Y.; Bian, J.; Pei, J. *Chem. Mater.* **2012**, *24*, 1762−1770.
(33) Rieger, R.; Beckmann, D.; Mavrinskiy, A.; Kastler, M.; Müllen, K. *Chem. Mater.* **2010**, *22*, 5314−5318.
(34) Yuan, J.; Huang, X.; Zhang, F.; Lu, J.; Zhai, Z.; Di, C.; Jiang, Z.; Ma, W. *J. Mater. Chem.* **2012**, *22*, 22734−22742.
(35) McCulloch, I.; Heeney, M.; Bailey, C.; Genevicius, K.; MacDonald, I.; Shkunov, M.; Sparrowe, D.; Tierney, S.; Wagner, R.; Zhang, W.; Chabinyc, M. L.; Kline, R. J.; McGehee, M. D.; Toney, M. F. *Nat. Mater.* **2006**, *5*, 328−333.
(36) Patra, D.; Sahu, D.; Padhy, H.; Kekuda, D.; Chu, C.-W.; Lin, H.-C. *J. Polym. Sci., Part A: Polym. Chem.* **2010**, *48*, 5479−5489.
(37) Wang, M.; Silva, G. L.; Armitage, B. A. *J. Am. Chem. Soc.* **2000**, *122* (41), 9977−9986.
(38) Kasha, M. *Radiat. Res.* **1963**, *20*, 55−70.
(39) Rieger, R.; Beckmann, D.; Pisula, W.; Steffen, W.; Kastler, M.; Müllen, K. *Adv. Mater.* **2010**, *22*, 83−86.